

## IMECE2009-12985

### REDUCED ORDER MODELING OF ENTRAINED FLOW SOLID FUEL GASIFICATION

Rory F.D. Monaghan, Mayank Kumar, Simcha L. Singer, Cheng Zhang, Ahmed F. Ghoniem

Massachusetts Institute of Technology, Reacting Gas Dynamics Laboratory, Department of Mechanical Engineering,  
Cambridge, MA 02139, USA

#### ABSTRACT

Reduced order models that accurately predict the operation of entrained flow gasifiers as components within integrated gasification combined cycle (IGCC) or polygeneration plants are essential for greater commercialization of gasification-based energy systems. A reduced order model, implemented in Aspen Custom Modeler, for entrained flow gasifiers that incorporates mixing and recirculation, rigorously calculated char properties, drying and devolatilization, chemical kinetics, simplified fluid dynamics, heat transfer, slag behavior and syngas cooling is presented. The model structure and submodels are described. Results are presented for the steady-state simulation of a two-metric-tonne-per-day (2 tpd) laboratory-scale Mitsubishi Heavy Industries (MHI) gasifier, fed by two different types of coal. Improvements over the state-of-the-art for reduced order modeling include the ability to incorporate realistic flow conditions and hence predict the gasifier internal and external temperature profiles, the ability to easily interface the model with plant-wide flowsheet models, and the flexibility to apply the same model to a variety of entrained flow gasifier designs. Model validation shows satisfactory agreement with measured values and computational fluid dynamics (CFD) results for syngas temperature profiles, syngas composition, carbon conversion, char flow rate, syngas heating value and cold gas efficiency. Analysis of the results shows the accuracy of the reduced order model to be similar to that of more detailed models that incorporate CFD. Next steps include the activation of pollutant chemistry and slag submodels, application of the reduced order model to other gasifier designs, parameter studies and uncertainty analysis of unknown and/or assumed physical and modeling parameters, and activation of dynamic simulation capability.

#### INTRODUCTION

Carbon dioxide capture and storage (CCS) is recognized as one of a suite of technology options that can be used to reduce greenhouse gas (GHG) emissions from continued fossil fuel usage [1-3]. Several approaches to carbon dioxide (CO<sub>2</sub>) capture, the most expensive step in CCS, have been suggested, among them, pre-combustion CO<sub>2</sub> capture systems, which employ gasification. Applications of gasification-based energy systems include IGCC plants for the production of power, and polygeneration plants for the production of industrial chemicals, fuels, hydrogen, and potentially power.

There are three general families of commercial gasifier designs: fixed/moving bed, fluidized bed and entrained flow. According to the DOE/NETL 2007 Gasification Database, nearly all planned gasifiers will be of the entrained flow family [4]. The primary

reasons for this are: high throughputs, high carbon conversions and very low concentrations of tars and hydrocarbons associated with entrained flow gasifiers (EFGs) [5]. Important characteristics of the main EFG designs are shown in Table 1. However, there are significant technical challenges associated with the operation of EFGs. Foremost among these are:

1. Lack of dynamic feedstock flexibility: changes in feedstock composition can lead to unacceptable syngas composition changes and unpredictable slag behavior.
2. Injector failure: high flame temperature and high particle velocities lead to short injector life. This is particularly true for slurry-fed designs.
3. Slag behavior: even under normal operating conditions, slag can freeze, causing corrosion and blockages inside the gasifier.

- Refractory failure: corrosion due to slagging, high temperatures and high particle velocities lead to premature refractory failure.
- Poor space efficiency: inadequate understanding of the internal flow fields leads to “dead zones”, which are of no use to conversion.
- Fouling and poisoning of downstream equipment: fly ash, sulfur compounds and unconverted carbon can damage downstream heat transfer surfaces, catalysts and turbomachinery.
- Poor plant integration: IGCC and polygeneration plants are extremely complex, and in many cases, individual plant components are not optimized for overall plant configuration.

**Table 1: Entrained flow gasifier characteristics**

Process	E-GAS	GE	MHI	OMB	PREN-FLO	SCGP	SFG
Vendor	CoP	GE	MHI	ECUST	Uhde	Shell	Siemens
Injectors	Opposed	Axial	Radial	Opposed	Radial	Radial	Axial
Flow	Up	Down	Up	Down	Up	Up	Down
Feed	Slurry	Slurry	Dry	Slurry	Dry	Dry	Dry
Oxidant	O <sub>2</sub>	O <sub>2</sub>	Air	O <sub>2</sub>	O <sub>2</sub>	O <sub>2</sub>	O <sub>2</sub>
Stages	Two	One	Two	One	One	One	One
Lining	Ref <sup>1</sup>	Ref	Mem <sup>2</sup>	Ref	Mem	Mem	Mem
Syngas cooling	Q <sup>3</sup>	Q or R <sup>4</sup> + Q	Q	Q	R + Q	R + Q	Q

Computer-based simulation is one method whereby improved gasifier designs and plant layouts can be analyzed and compared. The U.S. Department of Energy recognizes simulations as one of the most important steps to greater commercialization of gasification [6]. These models would ideally employ computational fluid dynamics (CFD) and extremely detailed submodels for the various physical, chemical and dynamic processes occurring inside the gasifier. Such detail, however, makes integration of these models with process flowsheet models of the overall IGCC or polygeneration plant difficult and impractical. For this reason, the work presented here focuses on the development of reduced order models (ROMs), which capture the most important processes of gasification, but without the computational expense of more detailed simulation. The ROM will primarily be used to simulate the interactions of the gasifier with the rest of the IGCC or polygeneration plant, i.e. we seek to address points 1, 6 & 7 above.

Reduced order modeling involves the representation of the gasifier by a reactor network model (RNM). The RNM consists of idealized chemical reactors, including 0-D well-stirred reactors (WSRs or CSTRs) and 1-D plug flow reactors (PFRs). The appropriate use of 0-D and 1-D components in the RNM drastically reduces the computational expense of simulation compared to CFD. RNMs have been used for modeling EFGs since the 1970s [7-17]. The following trends are observable when reviewing the state-of-the-art in ROMs:

- All of these studies use a combination of WSRs and PFRs in series, in essence assuming fully 1-D axial flow. With the exception of Smith and Smoot [10], no consideration is given to mixing and recirculation.
- With the exception of Bockelie et al. [15], none of the studies consider the fate of ash/slag in the gasifier.

<sup>1</sup> Ref: Refractory-lined

<sup>2</sup> Mem: Membrane-lined. Membrane refers to the metallic wall used in gasifiers that employ heat removal via steam. This lining design relies on the formation of a slag layer to protect the metallic wall from the harsh environment within the gasifier.

<sup>3</sup> Q: Quench cooling

<sup>4</sup> R: Radiant cooling

- With the exception of Vamvuka et al. [13, 14], all of the studies apply arbitrary or unknown temperature boundary conditions on the gasifier walls.
- While some of the studies track the formation of sulfur-based pollutants, none do so for nitrogen-based pollutants.
- None of the current models are capable of dynamic simulation.
- With the exception of Bockelie et al. [15], all of the studies focus on one gasifier design. Some studies do not validate their models against experimental results.

From a review of the state-of-the-art, it is clear that there is a need for ROMs that incorporate submodels for mixing and recirculation, slag behavior, heat loss through gasifier walls and pollutant formation. These submodels are required in addition to those already used in the previous studies, i.e. devolatilization, char conversion, particle properties, and chemical reactions. It is also important that these models are dynamic and validated for use over a range of commercial EFG designs. This paper describes the progress made towards developing a comprehensive ROM for integration with plant-wide process flowsheet models. Future papers will focus on modeling slag behavior, pollutant formation, dynamic gasifier operation, and the effect of uncertainty in physical and modeling parameters.

## MODEL DESCRIPTION

### The Reactor Network Model

Reactor Network Models (RNMs) are used to reduce the computational expense of gasifier simulation, compared to CFD-based models. It is therefore important to recognize the necessary differences between RNMs suitable for EFGs of vastly different design. The main design variation to consider when choosing an RNM is the number of firing stages of the gasifier. The next section describes an RNM for a one-stage gasifier. The subsequent section describes the modification of the one-stage RNM for use in a two-stage gasifier.

### One-Stage RNM

For modeling a one-stage gasifier we chose a reactor network model (RNM) developed by Pedersen et al. [18, 19]. A schematic of the flow in an axially-fired swirling coal combustor, for which the RNM was developed, as well as the RNM itself, is shown in Figure 1. It consists of four reactors or zones; two WSRs and two PFRs. Coal, oxidant and H<sub>2</sub>O (slurry or steam) enter at one end of the gasifier via swirl injectors. In the case of the slurry-fed GE gasifier for example, coal slurry is introduced via a central injector and oxygen enters via a swirling annular injector. In a reactor of this configuration, two recirculation zones are established; an internal recirculation zone (IRZ) and an external recirculation zone (ERZ).

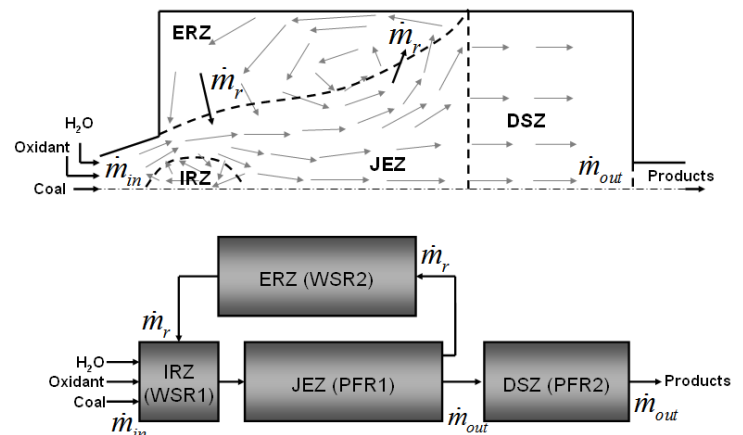


**Figure 1: Flow field and RNM for a one-stage gasifier**

Copyright © ASME 2009

## Flexible One- or Two-Stage RNM

The inlet streams mix vigorously with each other and with hot, recirculated gas and particles in the IRZ, which is represented by a WSR. To a first approximation, the structure of the IRZ may be considered to be governed primarily by the degree of swirl of the inlet streams. The precise inlet geometry and swirl conditions for most gasifiers are not known, so the assumption is made that the degree of swirl is sufficiently high to ensure full mixing of the inlet streams within a length of one quarl diameter from the gasifier inlet. The IRZ is therefore modeled as a cylinder of diameter and length  $d_{\text{quarl}}$ , where  $d_{\text{quarl}}$  is the diameter of the quarl. All inlet streams are assumed to fully pass through the IRZ.

The two-phase flow leaves the IRZ fully mixed and enters the jet expansion zone (JEZ), where the sudden expansion at the inlet of the gasifier causes the flow to spread out. The JEZ is represented by a truncated conical PFR. As the flow approaches the walls of the gasifier, detrainment from the expanding jet occurs and the flow splits into two streams. The portion of the flow that detrains from the jet flows back towards the IRZ through the external recirculation zone (ERZ), which is represented by a WSR.

To a first approximation, the structures of the JEZ and ERZ may be considered to be governed primarily by the geometry of the gasifier, and more specifically by the ratio of  $d_{\text{gasifier}}$  to  $d_{\text{quarl}}$ . Since the precise inlet geometry of the gasifiers under consideration are not known, the assumption is made that the quarl diameter is sufficiently small compared to that of the gasifier, so that the JEZ can be modeled as expanding as if it were a free jet.

The remainder of the flow leaving the JEZ, which does not enter the ERZ, proceeds to the reactor exit via a fully 1-D flow in the downstream zone (DSZ). In the original work by Pedersen et al, the DSZ was represented using a WSR. The present work uses a PFR as it is better able to simulate the relatively slow gasification reactions.

Three parameters are needed to use this RNM: the length of the IRZ ( $L_{\text{IRZ}}$ ), the jet expansion angle ( $\theta$ ) and the recirculation ratio ( $\alpha = \dot{m}_r / \dot{m}_m$ ). In this expression,  $\dot{m}_r$  and  $\dot{m}_m$  refer to mass flow rates of the recirculating and inlet streams, respectively. The present work evaluates these parameters in the same manner as Pedersen et al. [18, 19]. Therefore,  $L_{\text{IRZ}} = d_{\text{quarl}}$  is chosen, as described above. The jet expansion angle is increased by swirl and decreased by combustion. As discussed above, the JEZ is assumed to expand as if it were a free jet, so a value of  $9.7^\circ$  is chosen for  $\theta$ . This is the maximum observed jet expansion angle of a free jet (Chap. 2 in [20]). The recirculation ratio is evaluated using the method of Thring and Newby, where  $\alpha = 0.47(d_{\text{gasifier}}/d) - 0.5$  (Chap. 2 in [20]). In the Thring and Newby method,  $d$  is the characteristic diameter of the burner, which in this case is chosen as  $d = d_{\text{quarl}}$  [21]. The validity of these assumptions will be examined in future work using parameter studies.

Within each reactor or zone of the RNM, the ROM expresses mass, energy and momentum conservation equations in a fixed reference frame, treating solid and gas phases as pseudo-fluids. In addition to the conservation equations for the gas-solid flow in the gasifier, mass and energy balances are performed on the walls of the gasifier, to establish the wall temperature profile and slag layer thickness. The conservation equations for a 1-D PFR, as well as a legend explaining the terms used, are shown in Table 2. The same equations are applied to the WSRs, with  $\partial/\partial x$  terms replaced by  $1/L_{\text{WSR}}$ , where  $L_{\text{WSR}}$  is the length of a WSR. The RNM and the conservation equations were solved in Aspen Custom Modeler (ACM).

The one-stage RNM described above is insufficient for modeling two-stage gasifiers, such as the ConocoPhillips (CoP) or Mitsubishi Heavy Industries (MHI) gasifiers, which will be considered in this paper. Therefore the one-stage RNM is modified by the addition of an extra WSR, as shown in Figure 2. In this flexible RNM, the first stage of a two-stage gasifier (i.e. the combustor) is represented by a WSR, identified as the coal combustion zone (CCZ). In both the CoP and MHI designs, the first stage combustor is used to supply heat,  $\text{CO}_2$  and  $\text{H}_2\text{O}$  for the endothermic gasification reactions in the second stage gasifier (or reductor). Oxygen is supplied in such quantities as to fully oxidize the volatile components of the coal, but not consume all of the resulting char. Therefore the stream exiting the CCZ is assumed to consist only of  $\text{CO}_2$ ,  $\text{H}_2\text{O}$ ,  $\text{N}_2$ ,  $\text{SO}_2$  and unconverted char. The RNM employs a switch that can be used to stop the material and energy flows from the CCZ to the IRZ. This means that one-stage gasifiers, such as the GE, ECUST, Uhde, Shell and Siemens designs can easily be modeled with this RNM. The flexible one- or two-stage RNM is used for all modeling presented in this paper.

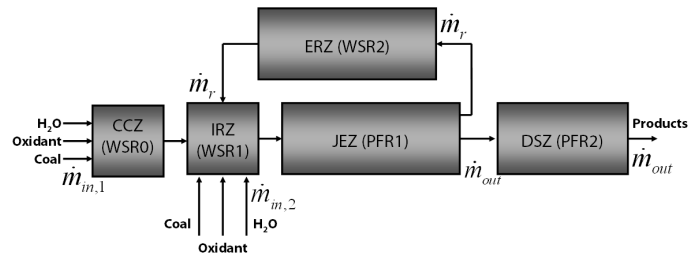


Figure 2: Flexible RNM for a one- or two-stage gasifier

## Model Implementation

As described above, mass, energy and momentum conservation equations are performed at every axial point in each of the PFRs, as well as for each WSR. In order to solve the equations presented in Table 2 it is necessary to evaluate all of the necessary variables. This is achieved through the use of submodels, which interact with the conservation equations and with each other. Each submodel receives estimated input variables from the conservation equations and/or other submodels, evaluates the required terms for the conservation equations, and sends them to the conservation equations. The ROM evaluates the error for the conservation equations and compares it to the tolerance (absolute residual) as defined by the ACM solver. For all conditions, the absolute residual is set to  $10^{-8}$ . If the error exceeds the tolerance, the ROM solves the conservation equations and the submodel equations iteratively.

Figure 3 shows the role of the submodels in the ROM. Variables that are passed between the conservation equations and submodels are shown by their symbols. The direction of information flow is indicated by the arrows. In addition to the variables evaluated by the submodels, fixed parameters, based on the design of the gasifier are provided. These include information on the gasifier geometry, and physical and thermodynamic properties for the wall layers. Input parameters, which describe the RNM and are discussed above, are also input. The flux of particles to the wall ( $\dot{m}'_{\text{slagging}}$ ) is not currently predictable by the ROM, and is set to a constant value for now. This is discussed further below. It is apparent from Figure 3 that the submodels interact with each other in a highly complex manner. Therefore it is necessary that great care is used in their development. The individual submodels are discussed in detail in the next section.

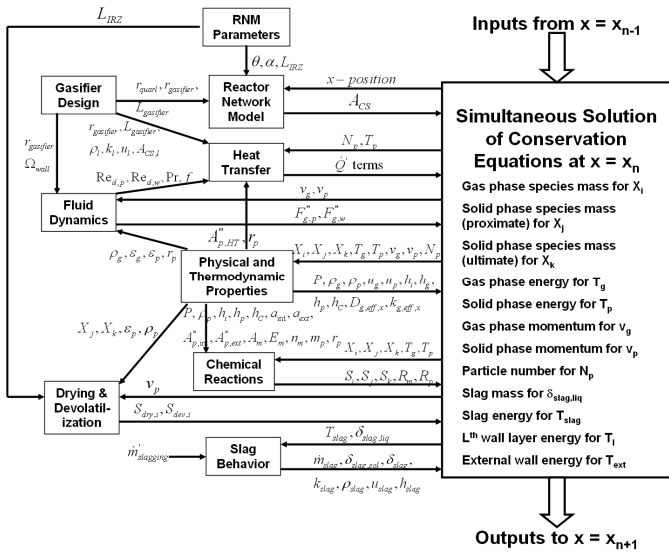


Figure 3: Model implementation using submodels

Table 2: Conservation equations for 1-D PFR

Conserved quantity	Expression	Variable solved for
Gas phase species mass	$\frac{\partial(A_{CS} X_i \rho_g \epsilon_g)}{\partial t} = \frac{\partial}{\partial x} \left( A_{CS} D_{g,eff,x} \frac{\partial(X_i \rho_g \epsilon_g)}{\partial x} \right) - \frac{\partial(A_{CS} v_g X_i \rho_g \epsilon_g)}{\partial x} + A_{CS} S_i$	$X_i$ (Gas phase mass fraction)
Solid phase species mass (proximate)	$\frac{\partial(A_{CS} \rho_p \epsilon_p X_j)}{\partial t} = - \frac{\partial(A_{CS} \rho_p \epsilon_p X_j v_p)}{\partial x} + A_{CS} S_j - \dot{m}'_{slagging} X_j$	$X_j$ (Solid phase proximate mass fraction)
Solid phase species mass (ultimate)	$\frac{\partial(A_{CS} \rho_p \epsilon_p X_k)}{\partial t} = - \frac{\partial(A_{CS} \rho_p \epsilon_p X_k v_p)}{\partial x} + A_{CS} S_k - \dot{m}'_{slagging} X_k$	$X_k$ (Solid phase ultimate mass fraction)
Gas phase energy	$\frac{\partial(A_{CS} \rho_g \epsilon_g u_g)}{\partial t} = \frac{\partial}{\partial x} \left( A_{CS} k_{g,eff,x} \frac{\partial T_g}{\partial x} \right) - \frac{\partial(A_{CS} \rho_g \epsilon_g h_g v_g)}{\partial x} + A_{CS} \left( \sum_i h_i (S_{dry,i} + S_{dev,i}) + \sum_m h_m R_m - h_C R_p \right) + \dot{Q}'_{conv,p \rightarrow g} - \dot{Q}'_{conv,g \rightarrow w}$	$T_g$ (Gas temperature)
Solid phase energy	$\frac{\partial(A_{CS} \rho_p \epsilon_p u_p)}{\partial t} = - \frac{\partial(A_{CS} \rho_p \epsilon_p h_p v_p)}{\partial x} - A_{CS} \left( \sum_i h_i (S_{dry,i} + S_{dev,i}) + \sum_m h_m R_m - h_C R_p \right) - \dot{Q}'_{conv,p \rightarrow g} - \dot{Q}'_{rad,p \rightarrow w} - \dot{Q}'_{rad,p \rightarrow p} - \dot{m}'_{slagging} h_p$	$T_p$ (Particle temperature)
Gas phase momentum	$\frac{\partial(A_{CS} \rho_g \epsilon_g v_g)}{\partial t} = - \frac{\partial(A_{CS} \rho_g \epsilon_g v_g^2)}{\partial x} + A_{CS} \left( - \frac{\partial P}{\partial x} + \rho_g \epsilon_g g - F_{g,w}'' - F_{g,p}'' \right)$	$v_g$ (Gas velocity)
Solid phase momentum	$\frac{\partial(A_{CS} \rho_p \epsilon_p v_p)}{\partial t} = - \frac{\partial(A_{CS} \rho_p \epsilon_p v_p^2)}{\partial x} + A_{CS} (\rho_p \epsilon_p g + F_{g,p}'')$	$v_p$ (Particle velocity)
Particle number	$\frac{\partial(A_{CS} N_p)}{\partial t} = - \frac{\partial(A_{CS} N_p v_p)}{\partial x} - \frac{\dot{m}'_{slagging}}{m_p}$	$N_p$ (Particle number density)
Slag mass	$2\pi r_{gasifier} \rho_{slag} \frac{\partial \delta_{slag}}{\partial t} = - \frac{\partial \dot{m}'_{slag}}{\partial x} + \dot{m}'_{slagging}$	$\delta_{slag}$ (Slag thickness)
Slag energy	$2\pi r_{gasifier} \rho_{slag} \frac{\partial(\delta_{slag} u_{slag})}{\partial t} = 2\pi r_{gasifier} k_{slag} \frac{\partial}{\partial x} \left( \delta_{slag} \frac{\partial T_{slag}}{\partial x} \right) - \frac{\partial(\dot{m}'_{slag} h_{slag})}{\partial x} + \dot{Q}'_{conv,g \rightarrow w} + \dot{Q}'_{rad,p \rightarrow w} - \dot{Q}'_{cond,slag \rightarrow w} + \dot{m}'_{slagging} h_p$	$T_{slag}$ (Slag Temperature)
$L^{\text{th}}$ wall layer energy	$\frac{\partial(A_{CS,l} \rho_l u_l)}{\partial t} = A_{CS,l} k_l \frac{\partial^2 T_l}{\partial x^2} + \dot{Q}'_{cond,l-1 \rightarrow l} - \dot{Q}'_{cond,l \rightarrow l+1}$	$T_l$ (Wall layer temperature)
External wall energy	$\frac{\partial(A_{CS,ext} \rho_{ext} u_{ext})}{\partial t} = A_{CS,ext} k_{ext} \frac{\partial^2 T_{ext}}{\partial x^2} + \dot{Q}'_{cond,ext-1 \rightarrow ext} - \dot{Q}'_{conv,ext \rightarrow amb} - \dot{Q}'_{rad,ext \rightarrow amb}$	$T_{ext}$ (External wall temperature)
Legend:	$h$ = Enthalpy $A_{CS}$ = Cross section area $D$ = Diffusivity $F''$ = Volumetric force $g$ = Gravitational acceleration $k$ = Conductivity $m$ = Mass $\dot{m}$ = Mass flow $\dot{m}'_{slagging}$ = Linear mass flux of particles to wall	$N_p$ = Number density of particles $P$ = Pressure $\dot{Q}'$ = Linear heat flux $R$ = Rate of chemical reaction $S$ = Chemical reaction source terms $T$ = Temperature $u$ = Internal energy $v$ = Velocity $X$ = Mass fraction $\rho$ = Density

## Submodels

### Physical and Thermodynamic Properties

Physical and thermodynamic properties for all gas phase species (with the exception of tar, which will be discussed later) are calculated using the Aspen Properties database. Solid phase properties are calculated according to the information in Table 3. Initial bulk particle density is assumed to be unknown and is calculated using Ergun and Menster's correlation based on dry, ash free hydrogen mole fraction ( $\hat{X}_{H,daf}$ ) [22]. Particle bulk density varies as char conversion occurs on internal and external particle surfaces. The particle density evolution parameter,  $\beta$ , is used to distinguish between conversion on external area (constant density) and internal area (constant radius). The density evolution parameter is described by  $\beta = \eta r_p A_{p,int} / V_p$ , where  $\eta$  is the effectiveness factor, which will be discussed later, and  $r_p$ ,  $A_{p,int}$  and  $V_p$  are the particle radius, internal surface area, and volume, respectively.

Merrick's model [23] is used to predict heat capacity and enthalpy as functions of coal composition and temperature. This allows the thermodynamic properties of the particle to change as devolatilization occurs. Thermodynamic properties of ash are predicted by Kirov's linear heat capacity model [24]. Ash enthalpy of fusion ( $\Delta h_{fus,ash}$ ) is chosen as 230 kJ/kg [25]. Particle internal energy is calculated by the thermodynamic relation  $u_p = h_p - P / \rho_p$ .

The random pore model (RPM) [26, 27] is used to model evolution of mass-specific internal particle area  $a_p$ , measured in terms of  $m^2/kg$ , as a function of carbon conversion ( $C$ ) and particle structural parameter ( $\psi$ ), while a fixed particle roughness ( $\Omega=5$ ) is used to calculate external area. Internal surface area evolution is tracked from the onset of devolatilization onwards. Liu's model is used to correlate post-devolatilization internal particle area as a function of initial proximate analysis [28]. The ROM submodels for chemical reaction and heat transfer require certain areas to be expressed as area per unit volume of reactor. These areas are the internal ( $A_{p,int}^*$ ) and external ( $A_{p,ext}^*$ ) particle areas, and the particle heat transfer area ( $A_{p,HT}^*$ ), all measured in terms of  $m^2/m^3$ . They are evaluated as described in Table 3 using the particle volume fraction,  $\varepsilon_p = N_p V_p$ .

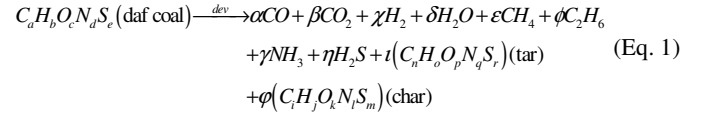
**Table 3: Calculated solid phase properties**

Property	Expression	Ref
Bulk density	$1 / \rho_p = X_{daf} / \rho_{daf} + X_M / \rho_M + X_{ash} / \rho_{ash}$	[22]
	$\rho_p = \rho_{p,0} (m_p / m_{p,0})^{\beta(1+\beta)}$ ; $\beta = \eta r_p A_{p,int} / V_p$	
	$\rho_{daf,0} = 1000 / (0.44 + 0.84 \hat{X}_{H,daf})$ ; $r_p = r_{p,0} (\rho_p / \rho_{p,0})^{-1/3} (m_p / m_{p,0})^{1/3}$	[29]
	$m_p = \rho_p V_p$ ; $V_p = 4\pi r_p^3 / 3$	
Enthalpy	$h_p = X_{daf} h_{daf} + X_M h_M + X_{ash} h_{ash}$	[23]
	$h_j(T) = h_{f,j} + \int_{T_0}^T c_{p,j} dT = h_{f,j} + h_{sens,j}$	
	$h_{sens,daf} = \mathfrak{R} / w_p (380 / (\exp(380/T) - 1) + 3600 / (\exp(1800/T) - 1) - 156)$	
	$h_{sens,ash} = 0.594(T - 298) + 0.293 \times 10^{-3} (T^2 - 298^2)$	[24]
Surface area	$a_p = a_{p,ext} + a_{p,int}$ ; $a_{p,ext} = 4\pi r_p^2 \Omega$	[26, 27, 28]
	$a_{p,int} = a_{p,int,0} (1 - C) \sqrt{1 - \psi \ln(1 - C)}$ ; $a_{p,int,0} = 10^3 (218.4 X_{VM} / X_{FC} + 98.4)$	
	$A_{p,int}^* = a_{p,int} \rho_p \varepsilon_p$ ; $A_{p,ext}^* = a_{p,ext} \rho_p \varepsilon_p$ ; $A_{p,HT}^* = a_{p,ext} \rho_p \varepsilon_p$	

### Drying and Devolatilization

During particle drying, all moisture is assumed to leave the particle upon heating. Volatile composition and yield is modeled using the Merrick model [30]. Rates of drying and devolatilization are not calculated as these processes are sufficiently fast (~1 ms) compared to the residence time of the particles in the CCZ or IRZ (~20 ms), where they are heated by volatiles combustion in excess  $O_2$  (CCZ), or

by recirculated gas and particles (IRZ). Therefore, all particles are assumed to be fully dried and devolatilized upon entering the JEZ. The products of devolatilization are: char,  $CH_4$ ,  $C_2H_6$ , CO,  $CO_2$ , tar,  $H_2$ ,  $H_2O$ ,  $NH_3$  and  $H_2S$ . Both char and tar products have compositions of the form  $C_\alpha H_\beta O_\gamma N_\delta S_\varepsilon$ .



All of the ash is assumed to remain in the char. In addition to five elemental balances for the global devolatilization process, the elemental compositions of char and tar are fixed, the yields of  $CH_4$  and  $C_2H_6$  are correlated to initial hydrogen content, and the yields of CO and  $CO_2$  are correlated to initial oxygen content. The final constraint on devolatilization is the correlation relating the actual volatiles yield to initial volatile matter (VM) content obtained by proximate analysis (ASTM D3172):  $Y_{daf,VM,act} = X_{daf,VM,0} - 0.36 X_{daf,VM,0}^2$ . The overall mass balance for Merrick's devolatilization model is shown in matrix form in Figure 4.

0.98	0.75	0.8	0.4286	0.2727	0.85	0	0	0	0	$X_{dev,Char}$	$X_{daf,CO}$
0.002	0.25	0.2	0	0	0.082	1	0.1111	0.1765	0.0588	$X_{dev,CH_4}$	$X_{daf,H_2O}$
0.002	0	0	0.5714	0.7273	0.049	0	0.8889	0	0	$X_{dev,C_2H_6}$	$X_{daf,CO}$
0.001	0	0	0	0	0.009	0	0	0.8235	0	$X_{dev,CO}$	$X_{daf,N_2}$
0.006	0	0	0	0	0.01	0	0	0	0.9412	$X_{dev,CO_2}$	$X_{daf,S,O}$
1	0	0	0	0	0	0	0	0	0	$X_{dev,Tar}$	$1 - Y_{VM,act}$
0	1	0	0	0	0	0	0	0	0	$X_{dev,H_2}$	$1.31 X_{daf,H_2O}$
0	0	1	0	0	0	0	0	0	0	$X_{dev,H_2O}$	$0.22 X_{daf,H_2O}$
0	0	0	1	0	0	0	0	0	0	$X_{dev,NH_3}$	$0.32 X_{daf,CO}$
0	0	0	0	1	0	0	0	0	0	$X_{dev,H_2S}$	$0.15 X_{daf,CO}$

**Figure 4: Mass balance for devolatilization submodel**

Since drying and devolatilization are assumed only to occur in the CCZ and/or IRZ, their source terms for the JEZ, ERZ and DSZ are all zero. Particles are fully dried and devolatilized upon leaving the IRZ, requiring the use of the following source term expressions in the CCZ and IRZ only.

#### Drying

For gas phase  $H_2O$ :  $S_{dry,H_2O} = \varepsilon_p \rho_p X_{M,0} v_p / L_{IRZ}$

For particle-bound moisture (M):  $S_{dry,M} = -S_{dry,H_2O}$

#### Devolatilization

For gas phase species:

$$S_{dev,i} = \varepsilon_p \rho_p Y_{daf,VM,act} X_{daf,0} X_{dev,i} v_p / (L_{IRZ} (1 - X_{dev,Char}))$$

For particle-bound volatile matter (VM):  $S_{dev,VM} = -\sum_i S_{dev,i}$

As previously stated, certain physical and thermodynamic properties for tar are calculated separately from the other gas phase species as tar does not exist in Aspen Properties. These include density, heat capacity and enthalpy. Tar is assumed to have similar properties, on a mass basis, to benzene ( $C_6H_6$ ) [9]. Therefore, when calculating molar properties of tar, it is necessary to scale the relevant properties of benzene by the ratio of the molecular weights, e.g.

$$\hat{h}_{tar} = \hat{h}_{C_6H_6} w_{tar} / w_{C_6H_6}, \text{ where } w_{tar} = 1 / \sum_k \hat{X}_k / w_k.$$

## Chemical Reactions

Chemical reactions appear in the mass conservation equations as source terms  $S_i$ ,  $S_j$  and  $S_k$  for gas phase, solid phase (proximate) and solid phase (ultimate) species, respectively. These source terms have units of  $\text{kg}/\text{m}^3/\text{s}$ . For gas phase species, which can participate in both homogeneous and heterogeneous reactions, the source term is defined as  $S_i = w_i(\sum_n v_{i,n} \hat{R}_n + 1/w_c \sum_m v_{i,m} R_m)$ , where  $\hat{R}_n$  is the rate of the  $n^{\text{th}}$  homogeneous reaction in units of  $\text{kmol}/\text{m}^3/\text{s}$  and  $R_m$  is the rate of the  $m^{\text{th}}$  heterogeneous reaction, both of which are described further in this section. The source terms for solid phase proximate and ultimate species are shown in Table 4. Since the proximate species all participate in different reactions, each source term is unique. Source terms for ash and moisture are obviously identical for both proximate and ultimate analyses. The source terms for the elemental coal constituents, C, H, O, N and S, are all identical due to the fact that all of these species undergo the same processes: devolatilization and heterogeneous chemical reaction.

**Table 4: Source terms for solid phase proximate and ultimate species**

Analysis	Solid phase specie	Source term
Proximate	Fixed carbon	$S_{FC} = -\sum_m R_m$
	Volatile matter	$S_{VM} = -\sum_t S_{dev,t} w_t$
	Ash	$S_{ash} = 0$
	Moisture	$S_M = -S_{dry}$
Ultimate	k = C, H, O, N, S	$S_k = S_{k,dev} w_k + X_{k,daf} S_{FC}$
	Ash	$S_{ash} = 0$
	Moisture	$S_M = -S_{dry}$

The global kinetics of homogeneous reactions for major species are modeled using rate expressions derived from Westbrook [31] and Jones [32]. Homogeneous reaction rate expressions of the form  $\hat{R}_n = k_n [\chi_1]^n [\chi_2]^{n_2}$ , and which have units of  $\text{kmol}/\text{m}^3/\text{s}$ , are shown in Table 5. Note that simulation convergence difficulties were encountered in ACM when  $k_n(T)$  was used for homogeneous reactions. For this reason, the values of  $k$  shown in Table 5 and used in the ROM are not functions of temperature for any homogeneous reaction, except the water-gas shift. For each homogeneous reaction, an average value of  $k_n$  was calculated over the expected temperature range inside the gasifier. Also, oxidation kinetics for  $\text{C}_2\text{H}_6$  and tar were assumed to be of the same form as that for  $\text{CH}_4$ . These simplifications do not affect the accuracy of the model as heterogeneous reaction kinetics are rate limiting under all realistic conditions.

**Table 5: Homogeneous reaction rate expressions**

Reaction	Rate expression	Ref
$\text{CO} + \frac{1}{2} \text{O}_2 \xrightarrow{k_1} \text{CO}_2$	$R_1 = 10^5 [\text{CO}] [\text{O}_2]^{0.25} [\text{H}_2\text{O}]^{0.5}$	[31]
$\text{H}_2 + \frac{1}{2} \text{O}_2 \xrightleftharpoons[k_2]{k_3} \text{H}_2\text{O}$	$R_2 = 10^8 ([\text{H}_2]^{0.25} [\text{O}_2]^{1.5} - [\text{H}_2\text{O}] / K_1)$	[32]
$\text{CH}_4 + \frac{1}{2} \text{O}_2 \xrightarrow{k_3} \text{CO} + 2\text{H}_2$	$R_3 = 10^8 [\text{CH}_4] [\text{O}_2]^{1.25}$	[32]
$\text{CO} + \text{H}_2\text{O} \xrightleftharpoons[k_4]{k_4} \text{CO}_2 + \text{H}_2$	$R_4 = 2.75 \times 10^9 \exp(-10072/T) \times ([\text{CO}][\text{H}_2\text{O}] - [\text{CO}_2][\text{H}_2] / K_4)$	[32]
$\text{CH}_4 + \text{H}_2\text{O} \xrightarrow{k_5} \text{CO} + 3\text{H}_2$	$R_5 = 10^5 [\text{CH}_4] [\text{H}_2\text{O}]$	[32]
$\text{C}_2\text{H}_6 + \text{O}_2 \xrightarrow{k_6} 2\text{CO} + 3\text{H}_2$	$R_6 = 10^8 [\text{C}_2\text{H}_6] [\text{O}_2]^{1.25}$	
$\text{Tar} + \text{O}_2 \xrightarrow{k_7} \text{CO} + \text{H}_2 + \text{SO}_2 + \text{N}_2$	$R_7 = 10^8 [\text{Tar}] [\text{O}_2]^{1.25}$	

Heterogeneous reaction kinetics are modeled using  $n^{\text{th}}$ -order rate expressions. Kinetic data may be input into the ROM in one of two forms; intrinsic or extrinsic. Intrinsic kinetic data results in the

calculation of an intrinsic reaction rate constant for the  $m^{\text{th}}$  reaction,  $k_{in,m} = A_{in,m} \exp(E_{in,m} / \mathcal{R}T)$ , with units of  $\text{kg}/\text{m}^2/\text{bar}^n/\text{s}$ . The area over which this reaction occurs is the total particle area available for reaction, so the reaction rate ( $\text{kg}/\text{m}^3/\text{s}$ ) is expressed as  $R_m = k_{in,m} (A_{p,ext}^m + \eta_m A_{p,int}^m) P_{s,m}^{n_{in,m}}$ . Expressions for the evaluation of the internal and external surface are presented in Table 3. The effectiveness factor ( $\eta_m$ ) will be discussed later. Very few sources of high pressure intrinsic kinetic data exist for the gasification reactions. An example of this type of data is the work of the Cooperative Research Centre for Coal in Sustainable Development (CCSD), Australia [33].

Due to the lack of intrinsic data, extrinsic data, which lump the effects of film diffusion, pore diffusion and chemical kinetics into a single expression, can also be used in the ROM. Extrinsic data results in the calculation of an extrinsic reaction rate constant for the  $m^{\text{th}}$  reaction,  $k_{ex,m} = A_{ex,m} \exp(E_{ex,m} / \mathcal{R}T)$ , with units of  $1/\text{bar}^n/\text{s}$ . The reaction rate ( $\text{kg}/\text{m}^3/\text{s}$ ) is therefore expressed as  $R_m = k_{ex,m} (\rho_{p,0} \epsilon_{p,0} a_{p,int} / a_{p,int,0}) P_{s,m}^{n_{ex,m}}$ . The modeling performed in this paper uses high pressure extrinsic data for two bituminous coals (Coal M and Coal T) developed by Kajitani et al. [34]. Frequency factors for both coals ( $A_{ex,m}$ ) are scaled relative to those of an Australian bituminous coal (Coal NL). The specifications of Coals M, T and NL are shown in Table 6, while the heterogeneous rate parameters of Coal NL are shown in Table 7. Note that different extrinsic parameters are used for low temperature (kinetic control) and high temperature (diffusion control).

**Table 6: Specifications of coal used in reduced order modeling**

Analysis		Coal M	Coal T	Coal NL	
Proximate	Fixed carbon	wt%	56.20	35.80	55.60
	Volatile matter	wt%	30.90	46.80	27.80
	Ash	wt%	8.70	12.10	13.40
Ultimate	Moisture	wt%	4.20	5.30	3.20
	C	wt%	73.10	64.59	68.80
	H	wt%	5.09	5.41	4.26
	O	wt%	7.00	11.61	8.87
	N	wt%	1.48	0.94	1.13
	S	wt%	0.44	0.18	0.35
	Ash	wt%	8.70	12.10	13.40
	Moisture	wt%	4.20	5.30	3.20
Scaling factor for $A_{ex,m}$			1.06	1.45	1.00

**Table 7: Kinetic rate parameters for Coal NL**

Reactant	$\text{O}_2$		$\text{H}_2\text{O}$		$\text{CO}_2$			
	Temp. range	$^\circ\text{C}$	< 1260	> 1260	< 1200	> 1200		
$\psi$			14	3	3	3		
$A_{ex,m}$			$10^6/\text{MPa}^n/\text{s}$	136	289	0.0855	334	0.0678
$E_{ex,m}$			MJ/kmol	130	252	140	271	163
$n_{ex,m}$				0.68	0.64	0.84	0.54	0.73

For the char oxidation reaction, a mechanism factor ( $\phi$ ) is used to account for direct conversion of carbon to  $\text{CO}_2$  at low temperatures. It is evaluated as follows [9]:

$$\text{For } r_p < 25 \times 10^{-6} \text{ m; } \phi = (2Z + 2) / (Z + 2)$$

$$\text{For } 25 \times 10^{-6} \text{ m} \leq r_p \leq 0.5 \times 10^{-3} \text{ m; } \phi = \frac{(2Z + 2) - Z(200r_p - 0.005) / 0.095}{Z + 2} \quad (\text{Eq. 2})$$

$$\text{For } r_p > 0.5 \times 10^{-3} \text{ m; } \phi = 1.0$$

$$\text{Where: } Z = [\text{CO}] / [\text{CO}_2] = 2500 \exp(-6249 / T_f)$$

When using intrinsic kinetic data, the partial pressure of each reactant at the particle surface ( $P_{s,m}$ ) is found by estimating its diffusion through a boundary layer around the particle:  $\dot{n}_i^* = \lambda_i(P_i - P_{s,i}) + P_{s,i} \sum \dot{n}_i^*$ , where the molar flux of each gas phase specie to the particle surface is given by  $\dot{n}_i^* = -a_p / (A_p^* w_i) \sum_m v_{i,m} R_m$

[35]. The heterogeneous reaction and particle boundary layer diffusion equations must be solved simultaneously. The effectiveness factor ( $\eta_m$ ) for each heterogeneous reaction is evaluated from the Thiele modulus ( $\phi_m$ ) as shown below [33]. As can be seen below, Thiele modulus is a measure of the relative rates of heterogeneous reaction to diffusion for a particle. Kinetic-controlled reactions result in effectiveness factors close to unity, while diffusion-control reactions give values near zero. Moreover,  $D_{i,eff,p}$ ,  $D_{i,A}$  and  $D_{i,K}$  refer to the effective, molecular and Knudsen diffusivities, respectively, of gas phase specie  $i$ .

$$\begin{aligned} \eta_m &= 3 / \phi_m (1 / \tanh \phi_m - 1 / \phi_m) \\ \phi_m &= r_p / 3 \sqrt{(n_m + 1) k_m \rho_p v_{i,m} a_p \mathcal{R} T_g P_{s,m}^{n_m - 1} / (2 w_c D_{i,eff,p})} \\ D_{i,eff,p} &= \varepsilon / 2 (1 / D_{i,A} + 1 / D_{i,K})^{-1} \\ D_{i,K} &= 2 \times 10^6 r_{pore} / 3 \sqrt{8 \mathcal{R} T_g / (\pi w_i)} \end{aligned} \quad (\text{Eq. 3})$$

Evaluation of the intraparticle Knudsen diffusivity of the reactants is difficult as it requires knowledge of the internal structure of the particle. Assuming knowledge of the particle porosity ( $\varepsilon$ ), solution of the following two simultaneous equations yields a first order estimate of the average pore radius ( $r_{pore}$ ) of a particle modeled by the random pore model (RPM) [26, 27]. It should be recalled that when using extrinsic heterogeneous reaction data, knowledge of the internal particle structure is not required.

$$a_{int} = \pi r_{pore} l_{pore} (1 - r_{pore} \sqrt{\pi l_{pore} \rho_p / 3}) \quad (\text{Eq. 4})$$

$$\varepsilon = \pi r_{pore}^2 l_{pore} \rho_p (1 - 2 r_{pore} / 3 \sqrt{\pi l_{pore} \rho_p / 3}) \quad (\text{Eq. 5})$$

## Fluid Dynamics

As described above, macro-scale inlet stream mixing and flow recirculation are modeled using the Reactor Network Model (RNM) developed by Pedersen [18, 19]. One-dimensional gas-particle and gas-wall viscous interactions are approximated using drag coefficient ( $C_D$ ) and friction factor ( $f$ ) methods, respectively. Table 8 shows the expressions used to evaluate the viscous interaction terms. The gas-particle friction interaction ( $F_{g,p}^*$ ) can be positive or negative, depending on the relative velocities of gas and particle, hence the  $v_{slip} / |v_{slip}|$  term in the force expression. The gas-wall friction interaction ( $F_{g,w}^*$ ) is positive under all conditions.

**Table 8: Viscous interactions**

Viscous interaction	Force per unit volume (N/m <sup>3</sup> )	Ref
Gas-particle	$F_{g,p}^* = 3 \varepsilon C_D \rho_g \varepsilon_g^{-2.65} v_{slip}^2 / (8 r_p) v_{slip} /  v_{slip} $	[36]
	$C_D = 24 / \text{Re}_{d,p} (1 + 0.15 \text{Re}_{d,p}^{0.687})$	[37]
Gas-wall	$F_{g,w}^* = f \rho_g \varepsilon_g v_g^2 / (16 r_{gasifier})$ $1 / f^{0.5} = -2 \log_{10} (\Omega_{wall} / 7.4 r_{gasifier} + 2.51 / \text{Re}_{d,w} f^{0.5})$	[38]

## Heat Transfer

The heat transfer terms evaluated in the ROM are shown in Figure 5. The ROM is capable of simulating gasifiers with wall cooling (membrane-cooled) and without (refractory-lined). Conduction through the wall layers of the gasifier is modeled in the axial and radial directions. Intraparticle conduction is not considered due to the small particle sizes involved. Two forced convection terms (gas-to-particle and gas-to-wall), and one natural convection term (external wall-to-atmosphere) are considered. Nusselt numbers for gas-to-particle and gas-to-wall convection are calculated using  $Nu_{d,p} = 1.32 \text{Re}_{d,p}^{1/2} \text{Pr}^{1/3}$  (Eq. 4.75 in [39]) and the Petukhov equation:  $Nu_{d,w} = (f/8) \text{Re}_{d,w} \text{Pr} / (1.07 + 12.7(f/8)^{1/2} (\text{Pr}^{2/3} - 1))$  (Eq. 8.62 in [40]), respectively. The Nusselt number for external convection is evaluated using the Churchill and Chu equation:  $Nu_{ext} = \{0.825 + 0.387 \text{Ra}_{ext}^{1/6} / [1 + (0.492 / \text{Pr}_{ext})^{9/16}]^{8/27}\}^2$  (Eq. 9.26 in [40]).

Radiative heat transfer between particles is modeled using the radiation-as-diffusion (RAD) approximation [41, 42, 10]. The Rosseland equation is used to express radiation throughout the particle cloud as a function of particle radius, temperature and temperature gradient, as well as the absorption coefficient ( $K$ ) of the particle cloud.

$$\dot{Q}_{rad}^* = - \frac{64 \sigma T_p^3 r_p^2}{3K} \frac{\partial T_p}{\partial x} \quad (\text{Eq. 6})$$

The use of the RAD approximation requires  $KB > 3$ , where  $B$  is the characteristic dimension of the gasifier. This means that the particle cloud must be of sufficient optical thickness. Under all realistic EFG conditions, this requirement is met. For clouds of particles of the size of pulverized coal  $K = \pi r_p^2 N_p$ , where  $r_p$  and  $N_p$  are the particle radius and number density ( $1/\text{m}^3$ ), respectively. Radiation in the gas phase is neglected as preliminary analysis indicates the absorption coefficient for the gas phase is significantly lower than that for the particle cloud. Radiation between particles and wall assumes no reflection from the wall [10]. The ROM allows radiation heat transfer between adjacent zones of the RNM. Radiation on the external wall of the gasifier treats the environment as a black body.

For use in the energy conservation equations, heat transfer terms must be evaluated in terms of heat transfer rates per unit axial length, with units of (kW/m). The expressions for these terms are shown below.

$$\dot{Q}_{conv,p \rightarrow g}^* = A_{p,HT} A_{CS} h_p (T_p - T_g) \quad (\text{Eq. 7})$$

$$\dot{Q}_{conv,g \rightarrow w}^* = 2 \pi r_{gasifier} h_w (T_g - T_w) \quad (\text{Eq. 8})$$

$$\dot{Q}_{rad,p \rightarrow w}^* = 2 \pi r_{gasifier} \sigma \varepsilon_w (T_p^4 - T_w^4) \quad (\text{Eq. 9})$$

$$\dot{Q}_{rad,p \rightarrow p}^* = -\partial (\dot{Q}_{rad}^* A_{CS}) / \partial x \quad (\text{Eq. 10})$$

$$\dot{Q}_{cond,l \rightarrow l+1}^* = 2 \pi k_l (T_l - T_{l+1}) / \ln(r_{l+1} / r_l) \quad (\text{Eq. 11})$$

$$\dot{Q}_{conv,ext \rightarrow amb}^* = 2 \pi r_{ext} h_{ext} (T_{ext} - T_{amb}) \quad (\text{Eq. 12})$$

$$\dot{Q}_{rad,ext \rightarrow amb}^* = 2 \pi r_{ext} \sigma \varepsilon_{ext} (T_{ext}^4 - T_{amb}^4) \quad (\text{Eq. 13})$$

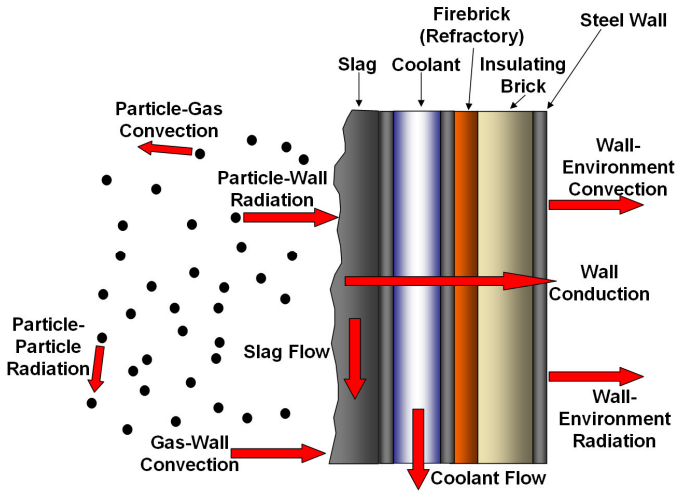


Figure 5: Heat transfer terms evaluated

### Slag Behavior

Slag behavior on the vertical gasifier walls is modeled in a similar manner to that employed by Seggiani [25]. Application of 1-D lubrication theory with temperature- and composition-dependent viscosity to a slag layer relates slag flow rate along the wall to slag layer thickness, via the following expression. Slag viscosity ( $\mu_{slag}$ ) is evaluated as a function of slag composition and temperature using the Urbain model [43]. In a review of slag viscosity models, the Urbain model, which is shown below, was recognized as one of the most suitable models for the reducing conditions encountered in gasifiers [44].

$$\dot{m}_{slag} = 2\pi r_{gasifier} \rho_{slag} \cos \beta \delta_{slag}^3 / (3\mu_{slag}(T_{slag})) \quad (\text{Eq. 14})$$

$$\mu_{slag}(T) = aT \exp(10^3/T)$$

$$\text{where} \quad -\ln a = 0.2693b + 13.9751 \quad (\text{Eq. 15})$$

$b$  is a complex empirical function of coal ash composition

The slag mass conservation equation provides an estimate of  $\dot{m}_{slag}$ , which is used to calculate a value for  $\delta_{slag}$ . The energy conservation equation provides an estimate of  $T_{slag}$ , which is used to calculate a value for  $\mu_{slag}$ . The ROM is not capable of predicting the flux of particles to the wall of the gasifier ( $\dot{m}_{slagging}$ ), so it must be specified as an input. For the current ROM,  $\dot{m}_{slagging}$  is set to a fixed value. Future versions will use  $\dot{m}_{slagging}$  predictions from CFD simulations.

### Syngas Cooling

Certain experimental data for operational gasifiers gives syngas composition for cooled, dry, sulfur-free (sweet) syngas. In order to compare the predicted composition of hot, raw syngas from the gasifier to the measured composition of sweet syngas, it is necessary to consider the method of syngas cooling employed. Note that in the case of the laboratory-scale MHI gasifier modeled in this paper, measurements were taken at the exit of the gasifier, not requiring the use of a syngas cooler. The following describes the manner in which the ROM models syngas cooling, despite the fact syngas cooling does not affect the results of this paper.

Syngas cooling is modeled using a 1-D PFR, with an integrated WSR, downstream of the downstream zone (DSZ) in the reactor network model (RNM). A switch in the cooler zone allows the

simulation of all possible syngas cooling options: radiant cooling only (PFR only), quench cooling only (WSR only), radiant and quench cooling (PFR and WSR in series), and no cooling (no PFR or WSR). The cooler zone allows the same physical and chemical processes to occur as the RNM does in the gasifier. Therefore all of the conservation equations identified in Table 2 are solved in the cooler zone. The ROM models a radiant syngas cooler (RSC) as a 1-D counter-flow heat exchanger. Saturated liquid water enters the cold end of the cooling tubes (water wall) at a prescribed pressure. The flow rate of cooling water is such that it is assumed to leave the water wall as a saturated vapor at the same pressure and temperature. The relatively slow cooling rate of syngas in commercial-scale operating RSCs (~100 K/s) allows the water-gas shift reaction to occur. This is in contrast to the rapid cooling rates associated with quench coolers (~30,000 K/s). Operational experience suggests that very little or no reaction occurs in quench coolers [15]. The ROM models a quench cooler as a vessel containing saturated H<sub>2</sub>O at the syngas pressure. Heat transfer between syngas and quench water is assumed to be sufficiently high to allow them to reach the same exit temperature. Energy conservation determines the quality of the quench water. The fraction of H<sub>2</sub>O in the vapor phase is assumed to leave the cooler with the syngas. The liquid water fraction leaves with solidified slag particles via the lock hopper.

### VALIDATION AND DISCUSSION

A ROM employing the RNM and submodels described above was constructed in Aspen Custom Modeler (ACM). The ROM was used to simulate the steady state performance of the 2 tonne-per-day laboratory-scale MHI gasifier operated by the Central Research Institute of the Electric Power Industry (CRIEPI) in Yokosuka, Japan [45, 46]. Like the commercial-scale MHI described in Table 1, the 2 tpd gasifier is fed with dry pulverized coal. No H<sub>2</sub>O, except for moisture present in the coal is supplied to the gasifier. The gasifier is air-blown, two-stage and up-flowing. The coal injectors are mounted radially in the combustor and reductor. The major difference between the 2 tpd and commercial-scale units is the fact that the reductor of the 2 tpd unit is refractory-lined, while that of the commercial-scale unit is membrane-cooled. A schematic of the gasifier and its design parameters are shown in Table 9.

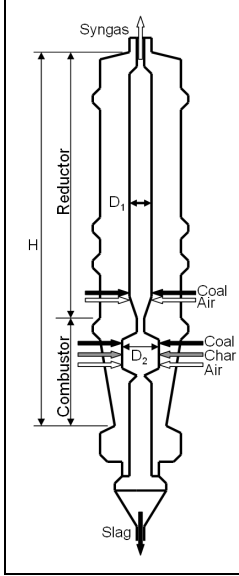
The ROM was validated by using it to simulate seven experiments that are described in detail by Watanabe [46]. The conditions for the seven tests are shown in Table 10. The model results were validated against the following experimental results and CFD simulations from Watanabe [46]: syngas temperature profiles, syngas composition, carbon conversion efficiency, char flow rate, syngas heating value and cold gas efficiency. Note the following definitions for terms used in the experiments, ACO and ACH refer to the stoichiometric flow rates of air with respect to coal and char flow rates, respectively.

$$\text{Air ratio: } \lambda_0 = \frac{\dot{m}_{air,total}}{(\dot{m}_{coal,combustor} + \dot{m}_{coal,reductor})ACO} \quad (\text{Eq. 16})$$

$$\text{Gasifier air ratio: } \lambda_g = \frac{\dot{m}_{air,total}}{(\dot{m}_{coal,combustor} + \dot{m}_{coal,reductor})ACO + \dot{m}_{char}ACH} \quad (\text{Eq. 17})$$



**Table 9: 2 tpd MHI gasifier schematic and design parameters**



Design parameter	Value	Source(s)
Overall height (H)	5.85 m	[45, 46]
Combustor height	1.71 m	Approx.
Reductor height	4.14 m	Approx.
Combustor diameter (D <sub>2</sub> )	0.30 m	[45, 46]
Combustor diameter (D <sub>1</sub> )	0.24 m	[45, 46]
Combustor walls	Water-cooled	[45, 46]
Reductor walls	Refractory-lined	[45, 46]
Firebrick (refractory)	0.16 m	Assumed
Insulating brick	0.06 m	Assumed
Steel wall thickness	0.02 m	Assumed
Firebrick (refractory) conductivity	2.4 W/m/K	[47] (Zirchrome 90)
Insulating brick conductivity	0.81 W/m/K	[47] (CA 333)
Steel wall conductivity	50 W/m/K	[40]
Pressure	2 MPa	[45, 46]
Firebrick (refractory) failure temperature	1800 °C	[47]

**Table 10: Test conditions**

Test		M-1	M-2	M-3	M-4	T-1	T-2	T-3
Input data								
Coal type		M	M	M	M	T	T	T
Pressure	MPa	2	2	2	2	2	2	2
Air ratio		0.469	0.495	0.525	0.476	0.463	0.488	0.525
Gasifier air ratio		0.358	0.381	0.409	0.367	0.392	0.463	0.506
Combustor coal	kg/hr	40.7	41.4	40.6	41.2	50.1	51.9	50.7
Reductor coal	kg/hr	60.3	59.3	58.3	61.3	52.2	49.6	50.5
Recycled char	kg/hr	38.1	36.3	34.8	37.8	33.6	9.8	7.7
Combustor air	kg/hr	391.7	418.4	436.6	409.7	342.0	365.4	371.8
Reductor air	kg/hr	66.96	66.58	66.49	66.68	61.9	65.1	66.3

### Syngas Temperature Validation

The results of reduced order modeling are shown in Figure 6 to Figure 12. Figure 6 and Figure 7 compare the experimentally recorded syngas temperature profiles for Coal M and Coal T, respectively, with the CFD predictions of Watanabe [46] and the ROM predictions performed in this paper. The flat sections of the ROM temperature profiles (a-b and c-d) indicate the location of the CCZ and IRZ, which are both WSRs. The steep drop in temperature (b-c) is the boundary between the CCZ, where combustion occurs, and the IRZ, where endothermic drying and devolatilization occur. The steep rise in temperature (d-e) is the result of rapid volatiles oxidation at the front end of the JEZ. The comparisons show satisfactory model accuracy in predicting syngas temperature profiles in the reductor of the gasifier (e-f), especially for Coal M. ROM accuracy in this region appears to be similar to that of the CFD model. For tests performed with Coal T, neither ROM nor CFD simulations predict the full extent of the flattening of the temperature profile. The ROM however, predicts the gasifier exit temperature to within 60 °C (point f).

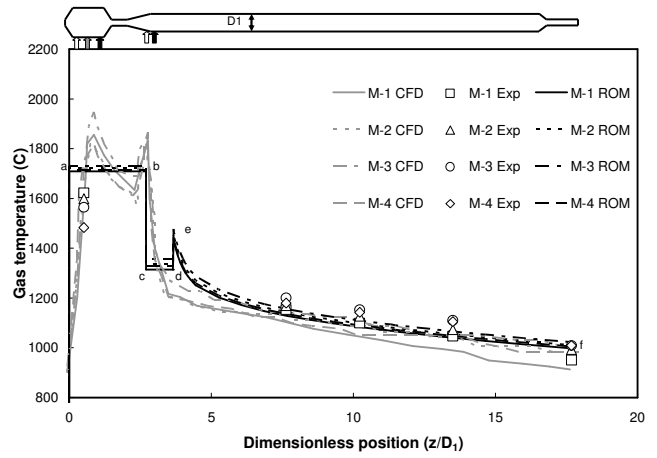


**Figure 6: Temperature profiles for tests with Coal M found by CFD, experiments and ROM**

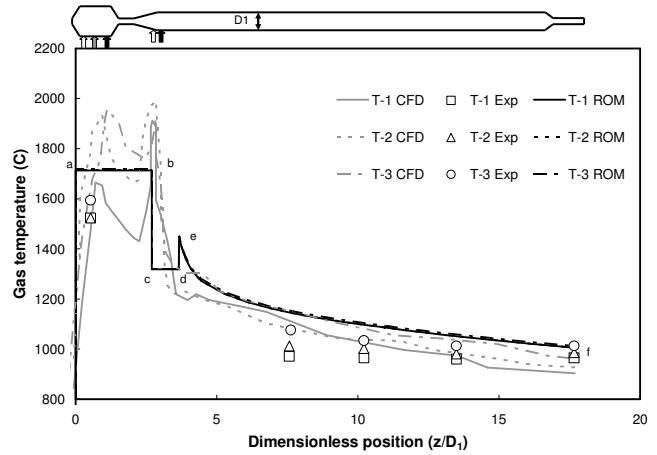


**Figure 7: Temperature profiles for tests with Coal T found by CFD, experiments and ROM**

### Syngas Composition Validation

Figure 8 compares the experimentally recorded syngas composition for all tests at the gasifier exit with the CFD predictions of Watanabe [46] and the ROM predictions performed in this paper. The primary syngas constituent in all cases is N<sub>2</sub> due to the fact that the MHI gasifier is air-blown. Nitrogen mole fraction for all cases is 55-60% and is not shown in Figure 8. The comparison shows ROM accuracy to be similar to that of the CFD model. It is important to note that for all tests, the gas phase exiting the gasifier is at chemical equilibrium. Differences between experiments and ROM and CFD predictions are due to differences in the predicted exit temperature as well as differences in stoichiometry due to predicted char reaction rates. One feature of note in Figure 8 is the ROM prediction of approximately constant H<sub>2</sub>O mole fraction over the range of tests. This has not yet been explained.

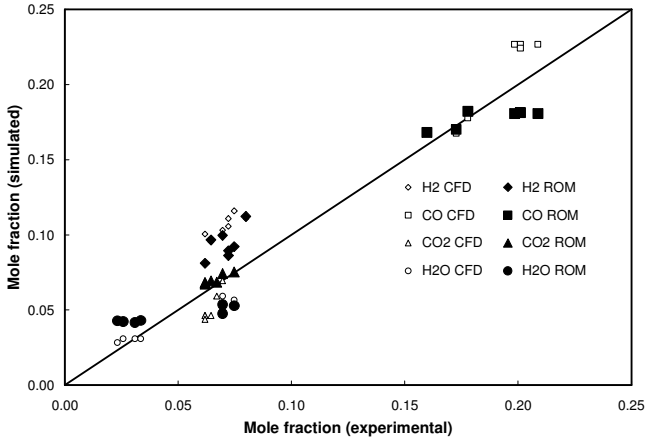


Figure 8: Syngas composition for all tests found by CFD, experiments and ROM

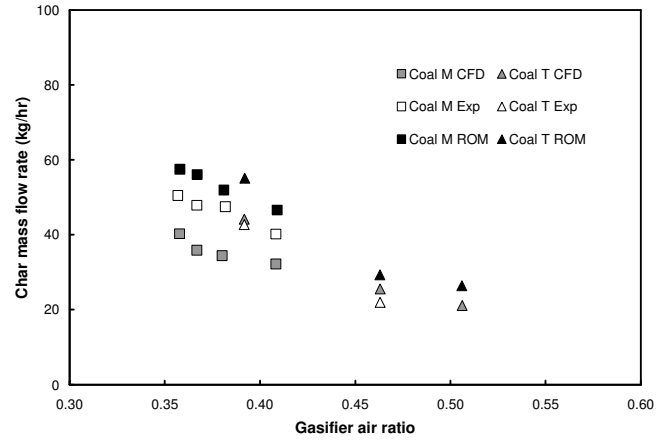


Figure 10: Char mass flow rate for all tests found by CFD, experiments and ROM

### Carbon Conversion and Char Flow Rate Validation

Figure 9 compares the experimentally recorded carbon conversion for all tests at the gasifier exit with the CFD predictions of Watanabe [46] and the ROM predictions performed in this paper. Because char recycle is employed in the MHI gasifier, carbon conversion is defined below. In the equation,  $\dot{m}_{C, gas, out}$  represents the mass flow rate of carbon contained in the gas phase at the gasifier exit. Since char is recycled, the carbon it contains is not considered an input for calculating conversion. Figure 9 shows that while the ROM slightly under-predicts carbon conversion, its accuracy appears to be similar to that of the CFD model.

$$C = \frac{\dot{m}_{C, gas, out}}{\dot{m}_{coal, combustor} X_{C, in} + \dot{m}_{coal, reductor} X_{C, in}} \quad (\text{Eq. 18})$$

Figure 10 compares the experimentally recorded char mass flow rate for all tests at the gasifier exit with the CFD predictions of Watanabe [46] and the ROM predictions performed in this paper. The ROM over-predicts char flow rate, which stands to reason as it also under-predicts carbon conversion. Again, a level of accuracy similar to that for CFD analysis was achieved by the ROM.

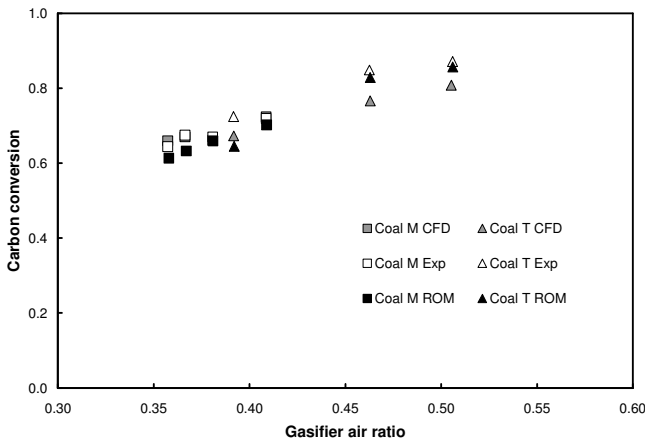


Figure 9: Carbon conversion for all tests found by CFD, experiments and ROM

### Syngas Heating Value and Cold Gas Efficiency Validation

Figure 11 compares the experimentally recorded syngas higher heating value (HHV) for all tests with the CFD predictions of Watanabe [46] and the ROM predictions performed in this paper. HHV is calculated on a dry, volumetric basis. The comparison shows that the ROM under-predicts syngas HHV, but is more accurate than the CFD model.

Figure 12 compares the experimentally recorded gasifier cold gas efficiency ( $CGE_{HHV}$ ) for all tests with the CFD predictions of Watanabe [46] and the ROM predictions performed in this paper.  $CGE_{HHV}$  is defined below. The comparison shows that the ROM slightly over-predicts  $CGE_{HHV}$  for all tests. Its accuracy, however, appears to be similar to that of the CFD model.

$$CGE_{HHV} = \frac{\dot{m}_{syngas} HHV_{syngas}}{(\dot{m}_{coal, combustor} + \dot{m}_{coal, reductor}) HHV_{coal}} \quad (\text{Eq. 19})$$

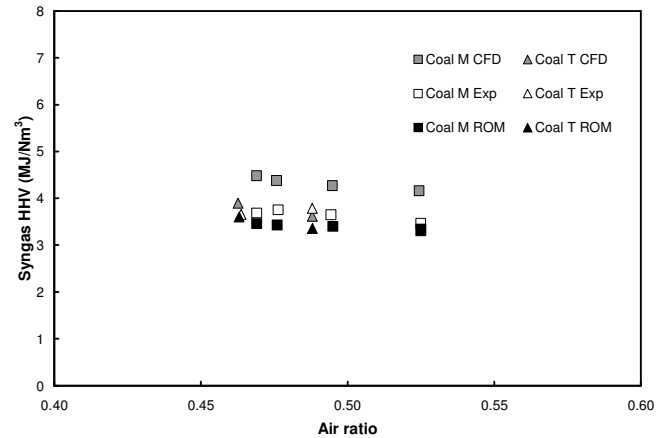
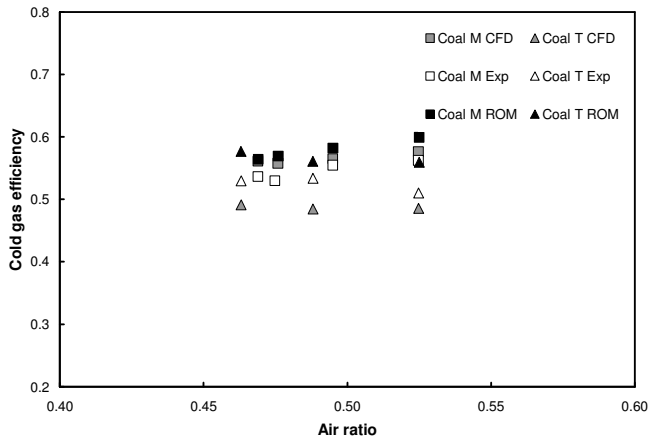


Figure 11: Syngas heating value for all tests found by CFD, experiments and ROM



**Figure 12: Cold gas efficiency for all tests found by CFD, experiments and ROM**

## CONCLUSIONS

A reduced order model (ROM) for simulation of entrained flow gasifiers (EFGs) is currently under development. The ROM was used to simulate the steady state performance of the 2 tpd laboratory-scale MHI gasifier operated by CRIEPI in Yokosuka, Japan. Model validation shows satisfactory agreement with measured values and CFD results for syngas temperature profiles, syngas composition, carbon conversion, char flow rate, syngas heating value and cold gas efficiency.

Flexible ROMs incorporating reactor network models (RNMs) are essential for better understanding the role of gasifiers in overall plant designs. Use of CFD-based models for this purpose would be unwieldy and inconvenient, given the length of time required for such simulations. The ROM, on the other hand, is capable of characterizing the steady-state performance of gasifiers in minutes. None of the test simulations presented in this paper took more than 5 minutes to converge. Further development of the ROM, however, will rely on parallel CFD modeling efforts currently underway in the Reacting Gas Dynamics Laboratory at MIT to supply modeling parameters. Examples of modeling parameters not predictable by the ROM include the geometry of the RNM and the flux of slag particles to the walls of the gasifier.

The next steps in ROM development are: the activation of pollutant chemistry and slag submodels, application of the ROM to other gasifier designs (see Table 1, as well as other laboratory-scale gasifiers such as those developed at CSIRO in Australia and ECUST in China), parameter studies and uncertainty analyses of unknown and/or assumed physical and modeling parameters (including the geometry and layout of the reactor network model), and activation of dynamic simulation capability (to simulate gasifier start-up, shutdown and fuel-switching).

## ACKNOWLEDGEMENTS

This research is funded by the BP-MIT Conversion Research Program. The authors wish to acknowledge Mr. Randall Field at the MIT Energy Initiative and Mr. James Goom at AspenTech for their assistance in developing the ROM in Aspen Custom Modeler.

## REFERENCES

- 1 Intergovernmental Panel on Climate Change [IPCC]. IPCC Special Report on Carbon Dioxide Capture and Storage. Prepared by Working Group III of the Intergovernmental

- Panel on Climate Change Cambridge, UK & New York, NY, USA: Cambridge University Press; 2005.
- 2 Massachusetts Institute of Technology [MIT]. The Future of Coal: options for a carbon-constrained world Cambridge, MA: 2007.
- 3 National Energy Technology Laboratory [NETL]. Cost and Performance Baseline for Fossil Energy Plants: Volume 1: Bituminous Coal and Natural Gas to Electricity. Revision 1 2007. DOE/NETL-2007/1281
- 4 National Energy Technology Laboratory [NETL]. Gasification Database: Active and Planned Commercial Gasification Plants 2007.
- 5 Shadle L J, Berry D A, Syamlal M. Coal Conversion Processes, Gasification. Kirk-Othmer Encyclopedia of Chemical Technology. Vol. 6. John Wiley & Sons, Inc.; 2002.
- 6 United States Department of Energy [U.S. DOE]. Gasification Technologies: Gasification Markets and Technologies – Present and Future – An Industry Perspective 2002 July. DOE/FE-0447
- 7 Ubhayakar S K, Stickler D B, Gannon R E. Modelling of Entrained-Bed Pulverized Coal Gasifiers, Fuel 1977; 56 (3): 281-291.
- 8 Stickler D B, Becker F E, Ubhayakar S K. Combustion of Pulverized Coal in High Temperature Preheated Air. American Institute of Aeronautics and Astronautics [AIAA]: 17th Aerospace Sciences Meeting; 1979 Jan. 15; New Orleans (LA): 1979, 79-0298
- 9 Wen C Y, Chung T Z. Entrainment Coal Gasification Modeling, Industrial and Engineering Chemistry Process Design and Development 1979; 18 (4): 684-695.
- 10 Smith P J, Smoot L D. One-Dimensional Model for Pulverized Coal Combustion and Gasification, Combustion Science and Technology 1980; 23: 17-31.
- 11 Govind R, Shah J. Modeling and Simulation of an Entrained Flow Coal Gasifier, AIChE Journal 1984; 30 (1): 79-92.
- 12 Phuoc T X, Durbetaki P. Pulverized Coal Conversion in Downflow Gasifier, International Journal for Numerical Methods in Engineering 1987; 24: 203-218.
- 13 Vamvuka D, Woodburn E T, Senior P R. Modeling of an entrained flow coal gasifier: 1. Development of the model and general predictions, Fuel 1995; 74 (10): 1452-1460.
- 14 Vamvuka D, Woodburn E T, Senior P R. Modeling of an entrained flow coal gasifier: 2. Effect of operating conditions on reactor performance, Fuel 1995; 74 (10): 1461-1465.
- 15 Bockelie M, Denison M, Chen Z, Senior C, Sarofim A. Using Models to Select Operating Conditions for Gasifiers. Pittsburgh Coal Conference; 2003 Sept. 15; Pittsburgh (PA): 2003
- 16 Uson S, Valero A, Correas L, Martinez A. Co-Gasification of Coal and Biomass in an IGCC Power Plant: Gasifier Modeling, International Journal of Thermodynamics 2004; 7 (4): 165-172.
- 17 Valero A, Uson S. Oxy-co-gasification of coal and biomass in an integrated gasification combined cycle (IGCC) power plant, Energy 2006; 31: 1643-1655.
- 18 Pedersen L S, Breithaupt P, Dam-Johansen K, Weber R. Residence Time Distributions in Confined Swirling Flames, Combustion Science and Technology 1997; 127 (1): 251-273.
- 19 Pedersen L S, Glarborg P, Dam-Johansen K, Hepburn P W, Hesselmann G. A Chemical Engineering Model for Predicting NO Emissions and Burnout from Pulverized Coal Flames, Combustion Science and Technology 1998; 132 (1): 251-314.

- 20 Beer J M, Chigier N A. Combustion Aerodynamics. London (UK): Applied Science Publishers, Ltd; 1972.
- 21 Smart J P, Woycenko, D M, Morgan, D J, van de Kamp, W L. Studies on Scale-Up of Swirl-Stabilised Pulverised-Coal Burners in the Thermal Range 2.5 – 12 MW, Journal of the Institute of Energy 1996; 69: 131-144.
- 22 Ergun S, Menster M. A Correlation between Helium Density and Hydrogen Content of Coals, Fuel 1960; 39: 509-510.
- 23 Merrick D. Mathematical models of the thermal decomposition of coal: 2. Specific heats and heats of reaction, Fuel 1983; 62: 540-546.
- 24 Kirov N Y. BCURA Monthly Bulletin 1965; 29: 33.
- 25 Seggiani M. Modelling and simulation of time varying slag flow in a Prenflo entrained-flow gasifier, Fuel 1998; 77 (14): 1611-1621.
- 26 Bhatia S K, Perlmutter D D. A Random Pore Model for Fluid-Solid Reactions: 1. Isothermal, Kinetic Control, AIChE Journal 1980; 26 (3): 379-386.
- 27 Bhatia S K, Perlmutter D D. A Random Pore Model for Fluid-Solid Reactions: 2. Diffusion and Transport Effects, AIChE Journal 1981; 27 (2): 247-254.
- 28 Liu G s, Tate A G, Bryant G W, Wall T F. Mathematical modeling of coal char reactivity with CO<sub>2</sub> at high pressures and temperatures, Fuel 2000; 79: 1145-1154.
- 29 Liu G s, Niksa S. Coal conversion submodels for design applications at elevated pressures. Part 2. Char gasification, Progress in Energy and Combustion Science 2004; 30: 679-717.
- 30 Merrick D. Mathematical models of the thermal decomposition of coal: 1. The evolution of volatile matter, Fuel 1983; 62: 534-539.
- 31 Westbrook C K, Dryer F L. Simplified Reaction Mechanisms for the Oxidation of Hydrocarbon Fuels in Flames, Combustion Science and Technology 1981; 27: 31-43.
- 32 Jones W P, Lindstedt R P. Global Reaction Schemes for Hydrocarbon Combustion, Combustion and Flame 1988; 73: 233-249.
- 33 Cooperative Research Centre for Coal in Sustainable Development [CCSD]. Gasification Conversion Model - PEFR: Research Report 80 2007 Dec.
- 34 Kajitani S, Hara S, Matsuda H. Gasification rate analysis of coal char with a pressurized drop tube furnace, Fuel 2002; 81: 539-546.
- 35 Hong J. Modeling char oxidation as a function of pressure using an intrinsic Langmuir rate equation [dissertation]. Provo (UT): Brigham Young University; 2000 Apr.. PhD thesis
- 36 Arastoopour H, Gidaspow D. Vertical Pneumatic Conveying Using Four Hydrodynamic Models, Industrial and Engineering Chemistry Fundamentals 1970; 18 (2): 123.
- 37 Rowe P N, Henwood G A. Drag Forces in Hydraulic Model of Fluidized Bed, Transactions of the Institution of Chemical Engineers 1961; 39: 43.
- 38 White F M. Fluid Mechanics, Second Edition. New York (NY): McGraw-Hill; 1986.
- 39 Mills A F. Heat Transfer, Second Edition. Upper Saddle River (NJ): Prentice Hall Inc.; 1999.
- 40 Incropera F P, DeWitt D P. Fundamentals of Heat and Mass Transfer, Fifth Edition. New York (NY): John Wiley & Sons, Inc.; 2002.
- 41 Hottel H C, Sarofim A F. Radiative Transfer. New York (NY): McGraw-Hill; 1967.
- 42 Smoot L D, Smith P J. Coal Combustion and Gasification. New York (NY): Plenum Press; 1985.
- 43 Urbain G, Cambier F, Deletter M, Anseau M R. Viscosity of Silicate Melts, Transactions of the Journal of the British Ceramics Society 1981; 80: 139.
- 44 Vargas S, Frandsen F J, Dam-Johansen K. Rheological properties of high-temperature melts of coal ashes and other silicates, Progress in Energy and Combustion Science 2001; 27: 237-429.
- 45 Hara S, Ichikawa K, Inumaru J, Ashizawa M. Examination of Gasification Characteristics of Pressurized Two-Stage Entrained Flow Coal Gasifier, JSME International Journal, Series B 2001; 44: 337.
- 46 Watanabe H, Otaka M. Numerical simulation of gasification in entrained flow coal gasifier, Fuel 2006; 85: 1935-1943.
- 47 Saint-Gobain Ceramics - Gasification [homepage on the Internet]. n.d. [cited 2009 May 11]. Available from: [http://www.refractories.saint-gobain.com/Data/Element/Node/Application/Application\\_edit.asp?ele\\_ch\\_id=A00000000000000001041](http://www.refractories.saint-gobain.com/Data/Element/Node/Application/Application_edit.asp?ele_ch_id=A00000000000000001041)
- 48 Watkinson A P, Lucas J P, Lim C J. A prediction of performance of commercial coal gasifiers, Fuel 1991; 70: 519-527.

## NOMENCLATURE

### Capital Letters

$A$	Area ( $m^2$ ) or Frequency factor ( $kg/m^2/atm^n/s$ )
$A^-$	Area per unit volume ( $m^2/m^3$ )
$ACH$	Stoichiometric ratio of air to char ( $kg/kg$ )
$ACO$	Stoichiometric ratio of air to coal ( $kg/kg$ )
$B$	Length scale for radiation heat transfer (m)
$C$	Particle conversion
$C_D$	Drag coefficient
$D$	Diffusivity ( $m^2/s$ )
$E$	Activation energy ( $kJ/kmol$ )
$F^-$	Viscous frictional force per unit volume ( $N/m^3$ )
$K$	Equilibrium constant or Absorption coefficient ( $m^{-1}$ )
$N$	Number density ( $m^{-3}$ )
$Nu$	Nusselt number
$P$	Pressure (Pa)
$\dot{Q}$	Heat transfer rate per unit axial length ( $kW/m$ )
$\dot{Q}^*$	Heat transfer rate per unit area ( $kW/m^2$ )
$R$	Rate of chemical reaction ( $kg/m^3/s$ )
$\hat{R}$	Rate of chemical reaction ( $kmol/m^3/s$ )
$\mathcal{R}$	Ideal gas constant ( $kJ/kmol/K$ )
Re	Reynolds number
$S$	Rate of species formation ( $kg/m^3$ ) or Swirl number
$T$	Temperature (K)
$V$	Volume ( $m^3$ )
$X$	Mass fraction ( $kg/kg$ )
$\hat{X}$	Mole fraction ( $kmol/kmol$ )
$Y$	Yield
$Z$	CO-CO <sub>2</sub> ratio at particle surface

### Lowercase Letters

$a$	Specific area ( $m^2/kg$ )
$a/b$	Acid-base ratio
$f$	Friction factor
$g$	Gravitational acceleration ( $m/s^2$ )
$h$	Enthalpy ( $kJ/kg$ ) or Heat transfer coefficient ( $kW/m^2/K$ )
$\hat{h}$	Enthalpy ( $kJ/kmol$ )
$k$	Conductivity ( $kW/m/K$ )

$k(T)$	Reaction rate constant ((kg/m <sup>2</sup> /atm <sup>n</sup> /s) for heterogeneous)
$l$	Length per unit mass (m/kg)
$m$	Mass (kg)
$\dot{m}$	Mass flow rate (kg/s)
$\dot{m}'$	Mass flow rate per unit axial length (kg/m/s)
$n$	Heterogeneous reaction order
$r$	Radius (m)
$s$	Silica ratio
$t$	Time (s) or Thickness (m)
$u$	Internal energy (kJ/kg)
$v$	Velocity (m/s)
$w$	Mole weight (kg/kmol)
$x$	Axial position (m)

### Greek Letters

$\alpha$	Recirculation ratio (kg/kg) or Slag viscosity ratio
$\beta$	Particle density evolution parameter or Solid slag surface
angle (deg)	
$\chi$	Chemical species
$\delta$	Thickness (m)
$\varepsilon$	Volume fraction (m <sup>3</sup> /m <sup>3</sup> ) or Porosity (m <sup>3</sup> /m <sup>3</sup> )
$\phi$	Mechanism factor or Thiele Modulus
$\eta$	Effectiveness factor
$\lambda$	Mass transfer coefficient (kmol/m <sup>2</sup> /s)
$\lambda_0$	Air ratio (kg/kg)
$\lambda_g$	Gasifier air ratio (kg/kg)
$\mu$	Viscosity (Pa.s)
$\theta$	Jet expansion angle (deg)
$\rho$	Density (kg/m <sup>3</sup> )
$\sigma$	Stefan-Boltzmann constant (5.67x10 <sup>-11</sup> kW/m <sup>2</sup> /K <sup>4</sup> )
$\nu$	Stoichiometric coefficient
$\Omega$	Particle roughness or Wall roughness (m)
$\psi$	Particle structural parameter

### Subscripts

A	Molecular diffusion
act	Actual
amb	Ambient
C	Carbon
cond	Conduction
conv	Convection
CV	Critical value (slag temperature)
dev	Devolatilization
d	Diameter
dry	Drying
eff	Effective
ex	Extrinsic
exit	Gasifier exit
ext	External
f	Formation or Film
fus	Fusion (heat of)
g	Gas
H	Hydrogen (elemental)
HT	Heat transfer
i	Gas phase species
in	Intrinsic
int	Internal
j	Solid phase species (proximate)
k	Solid phase species (ultimate)
K	Knudsen diffusion
l	Wall layer (i.e. firebrick (refractory), insulating brick, steel wall)
liq	Liquid

m	Heterogeneous reaction
M	Moisture
n	Homogeneous reaction
p	Particle
pore	Intraparticle pore
r	Recirculated
rad	Radiation
ref	Refractory
s	Particle surface
sens	Sensible
slag	Slag on wall
slagging	Slag transport to wall
sol	Solid
w	Wall
x	Axial direction
0	Initial or reference state

### Acronyms

ACM	Aspen Custom Modeler
CCS	Carbon dioxide Capture and Storage (or Sequestration)
CCSD	Cooperative Research Centre for Coal in Sustainable Development
CCZ	Coal Combustion Zone
CFD	Computational Fluid Dynamics
CGE	Cold Gas Efficiency
CoP	ConocoPhillips
CRIEPI	Central Research Institute of the Electric Industry
CS	Cross Section
CSTR	Continuously Stirred Tank Reactor (also WSR)
daf	Dry, Ash-Free (also dmmf: "dry, mineral matter free")
DOE	Department of Energy
DSZ	Downstream Zone
ECUST	East China University of Science and Technology
EFG	Entrained Flow Gasifier
ERZ	External Recirculation Zone
FC	Fixed Carbon
FB	Firebrick (refractory)
GE	General Electric
GHG	Greenhouse Gas
HHV	Higher Heating Value
IB	Insulating brick
IGCC	Integrated Gasification Combined Cycle
IRZ	Internal Recirculation Zone
JEZ	Jet Expansion Zone
MHI	Mitsubishi Heavy Industries
NETL	National Energy Technology Laboratory
OMB	Opposed Multi Burner
PFR	Plug Flow Reactor
PRENFLO	Pressurized Entrained Flow
RAD	Radiation-as-diffusion
RNM	Reactor Network Model
ROM	Reduced Order Model
RPM	Random Pore Model
RSC	Radiant Syngas Cooler
SCGP	Shell Coal Gasification Process
SFG	Solid Fuel Gasification
SUFCo	Southern Utah Fuel Company
TGA	Thermogravimetric analysis
tpd	Metric tonnes per day
VM	Volatile Matter
WGS	Water-Gas Shift
WSR	Well-Stirred Reactor (also CSTR)